applied sciences

MDPI

Article

Research on the Calculation and Analysis of Ski-Track Areas Based on Laser Point Clouds

Wenxin Wang [1,2,*,†,‡], Changming Zhao [1,2,†,‡] and Haiyang Zhang [1,2,†]

[1] Key Laboratory of Photoelectronic Imaging Technology and System, Ministry of Education, Beijing 100081, China
[2] Key Laboratory of Photonics Information Technology, Ministry of Industry and Information Technology, Beijing 100081, China
* Correspondence: 3120195308@bit.edu.cn
† Current address: School of Optics and Photonics, Beijing Institute of Technology, Beijing 100081, China.
‡ These authors contributed equally to this work.

Abstract: To address the long-term statistical problem of ski-track area in the construction and operation of ski resorts, we propose a new ski-track point cloud boundary extraction method that improves the accuracy of boundary extraction and minimizes the offset of the area error. In this method, all point clouds are first projected onto the fitting plane using the random sample consensus (RANSAC) method. An improved point cloud boundary extraction algorithm is used to triangulate and extract the high-precision ski-track boundary. A discrete Green formula is then used to calculate and count the ski track's exact area. It is demonstrated through five sets of test experiments that the error offset of the method proposed in this paper is smaller than that of other classical methods, which confirms its benefits and feasibility.

Keywords: laser point clouds; ski-track area; boundary extraction; discrete Green formula

check for updates

Citation: Wang, W.; Zhao, C.; Zhang, H. Research on the Calculation and Analysis of Ski-Track Areas Based on Laser Point Clouds. *Appl. Sci.* **2023**, *13*, 1632. https://doi.org/10.3390/app13031632

Academic Editor: Enrico Vezzetti

Received: 21 November 2022
Revised: 23 January 2023
Accepted: 24 January 2023
Published: 27 January 2023

Copyright: © 2023 by the authors. Licensee MDPI, Basel, Switzerland. This article is an open access article distributed under the terms and conditions of the Creative Commons Attribution (CC BY) license (https://creativecommons.org/licenses/by/4.0/).

1. Introduction

A complete set of surveying and mapping data is the most fundamental, direct, and reliable basis for the management of ski resorts, whether it is in the planning or maintenance stages [1–6]. There are several commonly used methods for surveying and mapping ski resorts, including ground surveys and remote-sensing estimations [7–11]. Typically, ground surveying is performed using a plumb line, tape measure, and other tools, which are not only costly, time-consuming, complicated, and destructive, but also have difficulty accurately recording the current situation of ski resorts due to limitations in measurement and expression. In spite of the fact that traditional remote-sensing estimation is capable of retrieving ski-resort parameters across a large area and has advantages in terms of time and space, it is limited to obtaining spectral information on the surface of ski resorts, and accuracy of measurement is low and difficult to achieve. As an active remote-sensing technology, lidar technology can obtain horizontal and vertical distribution information of the ski resort by emitting laser pulses with a certain penetration power to act on the ski slopes, vegetation and buildings of the ski resort, as well as recording and storing the information quickly [12–15]. The surface 3D point cloud data and the deep 3D structure data of the ski resort compensate for the limitations of traditional optical remote-sensing monitoring methods. As lidar technology has rapidly developed, 3D laser scanners have gradually evolved into a valuable tool for observing ski resorts from a distance, both near and far, and are increasingly being used in surveying and mapping various types of ski resorts because of their unique advantages [16,17].

Using a 3D laser scanner, a 3D digital reconstruction of the ski resort can be completed in a short period of time, a 3D model can be generated, and a map can be produced in a highly accurate and efficient manner. A comprehensive evaluation of ski-track quality

in ski resorts should take into account key indicators, such as ski-track thickness, slope, and area. A new research direction concerns the use of digital point cloud models to solve the ski-run area, since it is time-consuming and labor-intensive to calculate and analyze the area. Researchers at home and abroad have primarily used remote sensing to conduct area measurement research on ice and snow, vegetation, buildings, etc. There are two main types of measurement methods: 2D image detection and 3D point cloud measurement. The effective image data of the target area are primarily obtained with high-precision smart sensors, such as spaceborne or airborne imaging spectrometers, infrared cameras, and visible light cameras [18–20]. These image data are used to build a snow-cover model in order to examine snow volume, snow surface area, snow particle size and particle shape [21]. This method, based on the detection and measurement of two-dimensional images, is relatively simple and efficient, but it cannot be used to measure a specific target or location accurately. Additionally, this method of measurement is relatively ineffective and can only be used to update and monitor data on a daily basis. In terms of 3D point cloud measurement, the rapid acquisition of target features and the precise measurement of target areas are mainly carried out by means of airborne laser scanning (ALS), unmanned aerial laser scanning (ULS), terrestrial laser scanning (TLS) and mobile laser scanning (MLS) [22–24]. Nevertheless, the threshold selection standard is not clearly defined and the value of the threshold has a significant impact on the calculated surface area of the point clouds. Additionally, there are some third-party commercial software applications, such as Cyclone (developed by the German company Leic), that can estimate the target area. It is important to note, however, that this method has a low level of automation and often relies on regular graphics to estimate the target area, with a result that is often much larger than the actual value. In general, compared to other forms of surveying and mapping, the 3D laser scanner is an incredibly effective, high-precision, and easily accessible instrument for measuring ski slopes. In spite of this, the existing method of calculating area based on point cloud data faces the problems of a low degree of automation and a large deviation from the true value, which need to be addressed.

Considering the problems associated with area measurement using the above methods, the UAV-borne LiDAR system was selected as the main method of collecting data. Our paper proposes an improved algorithm for estimating ski-track point cloud boundaries based on the extracted ski-track point cloud data [25] (DOI: 10.3390/app12115678). The purpose of this method is to eliminate large gaps outside the ski run, extract the outer contour of the ski-run point cloud that is more in line with the actual situation, and to calculate accurate statistics on the ski-run area.

2. Ski-Track Data Pre-Processing

The best ski-track plane should be fitted in advance and all the point cloud data of the ski track should be projected onto the fitted plane to determine the edge of the ski track accurately to calculate the area.

Currently, least squares fitting is the most common and easiest method of fitting a plane; however, the accuracy of least squares fitting is easily affected by noise. With the random sampling consensus algorithm (RANSAC) [26], the influence of noise can be eliminated through an iterative fitting method, which greatly improves the accuracy of the fit. As shown in Figure 1, the flow of the random sampling consensus algorithm is as follows:

1. Based on mathematical knowledge, a plane can be fitted with at least three points, so, first, three points are randomly chosen and then the plane model parameters A, B, C, and D are calculated based on the plane Equation (1).

$$A \cdot x + B \cdot y + C \cdot z = D \tag{1}$$

2. As a result of testing the plane model estimated in Equation (1), the result error is calculated and the error is compared with the set error threshold. If the error is less than the set error threshold, then the point is considered an inner point and the number

of interior points under this parameter model is counted and recorded. Moreover, the distance threshold (T) and assurance (A) are set at 1 cm and 0.7, respectively, during the plane-fitting process.

3. Continue with steps 1 and 2. In the event that the number of inliers in the current model exceeds the maximum number of inliers saved, update the model parameters; the reserved parameters are always those with the most inliers.

4. Iterate continuously until the threshold is reached and then find the model parameters with the highest number of inliers. Then use the inliers to estimate the model parameters again to obtain the final parameters.

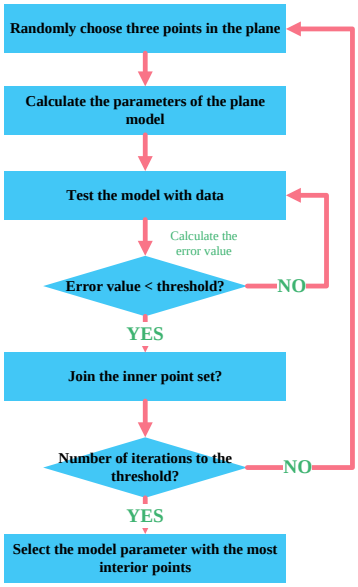

Figure 1. The flow of the random sampling consensus algorithm.

By using the derived projection formula, the projected point of any point cloud on the plane can be easily calculated using the characteristic that the projected vertical line is parallel to the fitted plane normal vector. As a result, the entire point cloud only needs to be projected onto the fitted ski-run plane by repeating the process. There is a large overlap between the final projected surface and the real ski run, so the projection surface can be approximated as the ski-run surface It is implemented in the PCL and can, therefore, be accessed directly during use.

3. Calculation of Ski Track Area

3.1. Construction of Triangulation Network Based on Growth Algorithm

A number of algorithms are available for the calculation of plane point sets, including the incremental method [27], the Graham scan method [28], the volume-wrapping method [29], and the divide-and-conquer method [30]. While Graham's algorithm is one of the most widely used and efficient algorithms, it is not capable of removing ski-track edge gaps with complex shapes and sizes. The purpose of this paper is to provide an improved method for determining point cloud boundaries, namely an improved growth algorithm, which is used to construct a triangular network using the plane point cloud obtained in Section 2, as shown in Figure 2. In addition, this paper shows that the RANSAC algorithm's time complexity for plane fitting is $O(n^2)$, while the improved growth algorithm's time complexity for triangular grid generation is $O(nlogn)$. A triangular network is constructed using the following growth algorithm:

1. The initial edge AB in the edge table is formed by taking the closest point B to the starting point A in all point cloud data, as shown in Figure 2.

2. Select a point C in the remaining point cloud data to maximize ∠ACB, then place the newly generated two edges AC and BC in the edge table, and place △ABC as the first

triangle in the triangle. Take any edge from the edge table and assume that it is a BC edge, then the BC edge will divide the plane into two half-planes. Find the discrete point D in the remaining point cloud data. The selection principle is to make the point D and point A different from the same half-plane of the BC side and to maximize ∠BDC. Add the new edges BD and CD to the edge table and △BCD to the triangle table.

4. Repeat step 3 until all point cloud data are processed.

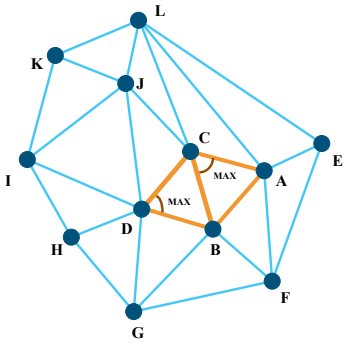

Figure 2. Triangulation network based on improved growth algorithm.

3.2. Point Cloud Boundary Extraction for Ski Tracks

In the Graham scanning method, the ski-track boundary is the smallest convex polygon containing all point clouds [31–37]. This polygon cannot show the details of the ski-track edge and retains the gap outside the ski track, preventing accurate calculation of the ski-track area. In view of the above problems, this paper proposes an improved ski-track point cloud boundary extraction algorithm. If the external gap of the ski-track point cloud data boundary is to be proposed, the outermost triangle filtering threshold needs to be set, and all external triangles are filtered in a clockwise manner. Whenever the side length of the external triangle exceeds the threshold, the triangle is considered to be an external gap and is eliminated. During the traversal of the irregular triangulation, the external triangle is gradually traversed from the outside to the inside. In the event that any side of the external triangle is less than the threshold, the search can be terminated. As a result of the search, there may be triangles whose side lengths exceed the threshold, which do not need to be removed. The cause of this phenomenon may relate to the intersection of ski runs. For the point cloud data density, it may be beneficial to retain these triangles in order to improve the stability of the ski-track point cloud boundary extraction algorithm. The original triangulation is shown in Figure 3a; the pink part of the triangulation represents the triangulation that needs to be optimized. The optimized triangulation is shown in Figure 3b. Implementation of the algorithm consists of the following steps:

1. To construct a 2D triangulation of the ski-track point cloud obtained by projection in Section 2, the growth algorithm described in Section 3.1 is applied.

2. A threshold of D is applied to the outermost triangle filtering and the outer triangles (i, i+1, . . .) are traversed from the outside to the inside of the irregular triangular network. The retrieval can be stopped if all the edges of the outer triangles are less than the threshold.

3. In order to preserve the coordinates of the endpoints of the outermost triangle, the corner points of each edge are retained in order according to the outer contour.

Based on the above-mentioned improved ski-track point cloud boundary extraction algorithm, the polygon formed by the boundary of each layer of point cloud is extracted. Based on the coordinates of the boundary endpoints, the discrete Green formula [38], as shown in Equation (2), is used to calculate the area of the polygon of the ski run.

$$\begin{aligned} S &= \frac{1}{2}\sum_{i=1}^{m}[x_i(y_{i+1}-y_i)-y_i(x_{i+1}-x_i)] \\ &= \frac{1}{2}\sum_{i=1}^{m}[x_iy_{i+1}-y_ix_{i+1}] \end{aligned} \tag{2}$$

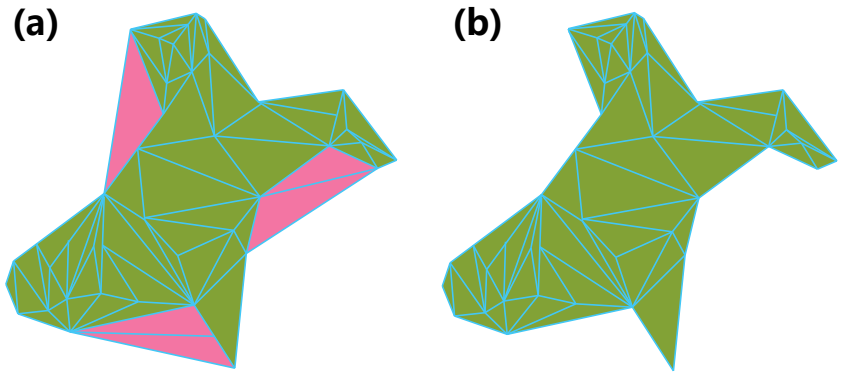

Figure 3. An analysis of the filtering effect of a triangular network: (**a**) represents the graph before filtering; (**b**) represents the graph after filtering.

Among these, S represents the total area of the extracted ski track, m represents the total number of points along the boundary of the ski track, (x_i, y_i) represents the plane projection coordinates of point i, and (x_{i+1}, y_{i+1}) represents the plane projection coordinates of point $i + 1$.

4. Experiment and Discussion

4.1. Data Collection

In the experimental verification stage, the unmanned aerial vehicle lidar system (including M600 Pro UAV, RIEGL VUX-1 UAV lidar, etc., which has completed integrated verification and data calibration) was used to collect point cloud data from the Zhangjiakou Wanlong Ski Resort and the National Cross-Country Skiing Center for the Beijing Winter Olympics. The unmanned aerial vehicle lidar system is shown in Figure 4a, and the collected point cloud data of the Wanlong Ski Resort and the National Cross-Country Skiing Center are shown in Figure 4b,c.

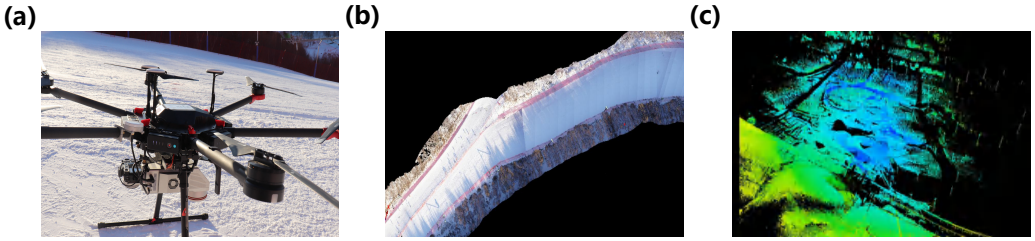

Figure 4. A UAV LiDAR system used to collect data: (**a**) represents the lidar system; (**b**) point clouds from the Wanlong Ski Resort; (**c**) point clouds from the National Cross Country Skiing Center.

In order to illustrate and verify the effectiveness of the proposed method, the point cloud data of the ski resort in Figure 4b,c are selected as experimental objects and the differences between the classical Graham algorithm and the method presented in this paper for the processing of dense and complex point clouds and sparse and simple point clouds are compared.

4.2. Triangular Network

As an example, the growth algorithm is used to construct a triangular network of ski-track point clouds, as shown in Figure 5. A comparison of Figure 5a,b shows that the boundary of the ski-run point cloud triangle network constructed by the growth algorithm and the boundary extracted by the Graham algorithm contain the same amount of ski-run edge gaps. The improved method described in this paper is used to establish a triangular network for the growth algorithm in order to accurately eliminate the outer gap of the ski run, as shown in Figure 6a; the extracted boundary can be seen in Figure 6b. According to Figures 5 and 6, the Graham algorithm extracts a larger boundary of the ski point cloud than

the filtering triangulation algorithm; however, the boundary extracted by the improved ski point cloud boundary extraction algorithm is closer to the edge contour of the actual slice point cloud as a result of the improved ski-track point cloud boundary extraction algorithm.

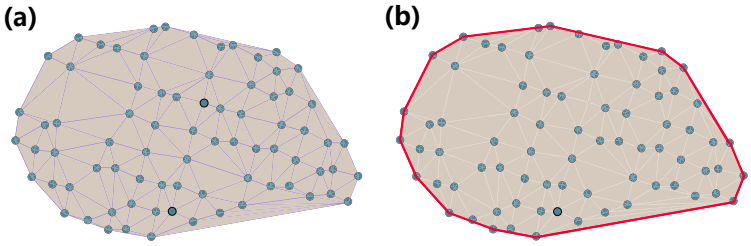

Figure 5. Triangulation generation and boundary extraction of dense point cloud based on Graham algorithm: (**a**) represents triangular mesh generation; (**b**) represents boundary extraction.

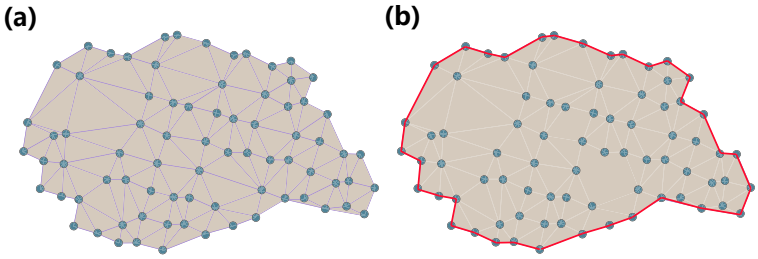

Figure 6. Triangulation generation and boundary extraction of dense point cloud based on proposed algorithm: (**a**) represents triangular mesh generation; (**b**) represents boundary extraction.

In contrast, if the point cloud of the ski track is sparse and simple, the Graham algorithm will surround the larger outer space. In this case, the area calculated by the Graham algorithm will be much larger than the actual area of the ski track, which will result in a much larger calculated area than the truth value. As shown in Figures 7 and 8, the improved ski-track point cloud boundary extraction algorithm eliminates the large external gap, resulting in an improved calculation of the ski-slope area.

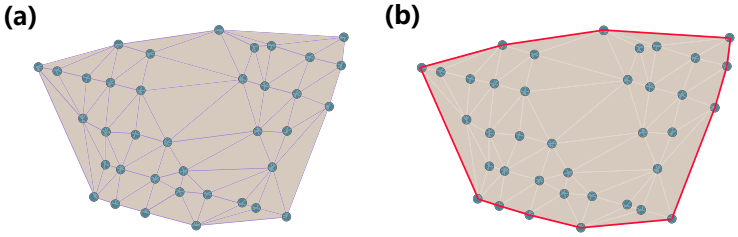

Figure 7. Triangulation generation and boundary extraction of sparse point cloud based on Graham algorithm: (**a**) represents triangular mesh generation; (**b**) represents boundary extraction.

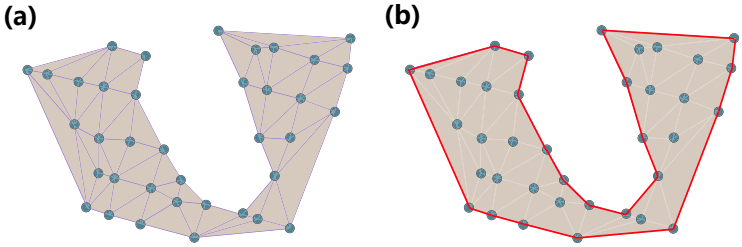

Figure 8. Triangulation generation and boundary extraction of sparse point cloud based on proposed algorithm: (**a**) represents triangular mesh generation; (**b**) represents boundary extraction.

4.3. Results and Analysis

Afterward, a visual comparison is conducted at the data level. The ski runs were divided into five test areas of 10 m × 5 m, as shown in Figure 9. Table 1 provides the

statistical results of the calculation and counting of the area of the measurement area using total stations and differential positioning equipment, the Graham algorithm, the concave hull algorithm, and the algorithm presented in this paper.

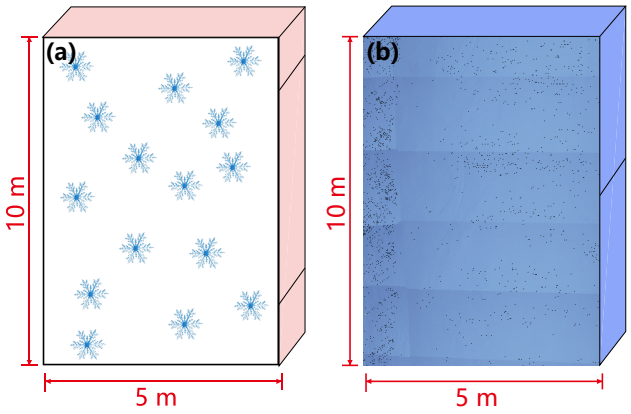

Figure 9. The selection of test area consists of two parts: (**a**) a schematic diagram of the sampling area; and (**b**) a real-time point cloud of the sampling area.

Figure 9 depicts a schematic diagram of the sampling area and the 3D point cloud image of the sampling area, with Figure 9a showing the schematic diagram and Figure 9b showing the real 3D point cloud image. Based on the coordinate information in Figure 9a, we can determine the actual range of the point cloud in Figure 9b. Additionally, this paper examines the accuracy and validity of the proposed method in comparison to other approaches. The standard measurement area of 10 m by 5 m is selected based on the total station and differential positioning equipment and other factors are ignored for subsequent calculations. In addition, the criteria for selecting samples from other test areas are the same.

Table 1. Statistical table of area of different measurement areas by different methods.

Test Area	Graham Algorithm/m^2	Concave Hull Algorithm/m^2	Proposed Algorithm/m^2	Standard Value/m^2
1	59.78	60.04	55.32	50.00
2	62.21	68.43	56.26	50.00
3	57.77	58.76	52.03	50.00
4	63.93	67.32	57.75	50.00
5	76.63	68.65	61.89	50.00

The results of Table 1 indicate that, using the existing method [25], ski-run point clouds can effectively be extracted from the five sample areas so that subsequent area calculations and statistics can be performed using the Graham measurement method, the concave hull measurement method, and the proposed method. By analyzing Table 1, together with performing simple calculations, it is evident that, although the calculation results for the three methods are larger than the standard value (as part of the point cloud extraction process, snow network information may be included, which will be improved in a targeted manner in the future), the error offsets are different. For each of the five groups of measurement areas, the Graham algorithm error offsets were +19.56%, +24.42, +15.54, +27.86% and 33.26%, respectively, and the average error was +24.13%. Based on the concave hull algorithm, the error offsets for the five groups of measurement areas were +20.08%, +36.86%, +17.52%, +34.64%, and +37.30%, respectively, with an average error of +29.28%. As a result of use of the proposed algorithm, the error offsets for the five groups of measurement areas were +10.64%, +12.52%, +4.06%, +15.50%, and +23.78%, respectively, with the average error being +13.30%. Furthermore, our algorithm achieved an average performance improvement of 10.83% with respect to the Graham algorithm and 15.98% with respect to the concave hull algorithm based on the experimental results. As shown by

the average error offset percentages for the three algorithms above, the method proposed in this paper had the lowest error offset and was closest to the real value, which indicates its true effectiveness.

Therefore, the method proposed in this article was employed to calculate and count the area of the extracted ski-track point cloud. The original point cloud images of each group of ski runs and the edge extraction renderings are shown in Figures 10–13.

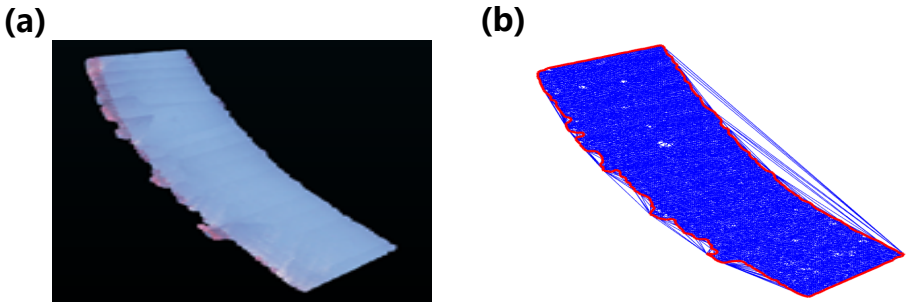

Figure 10. The first group of data-processing results for the Zhangjiakou Wanlong Ski Resort (Parameters: T = 1.2 cm, A = 0.7, D = 43 cm): (**a**) color point cloud; (**b**) ski-track boundary extraction.

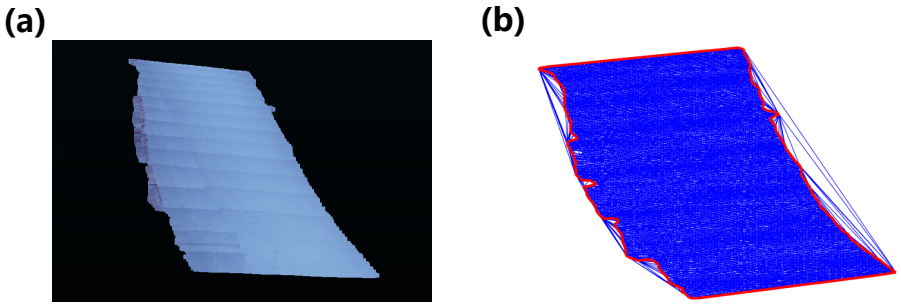

Figure 11. The second group of data-processing results for the Zhangjiakou Wanlong Ski Resort (Parameters: T = 1.8 cm, A = 0.7, D = 38 cm): (**a**) color point cloud; (**b**) ski-track boundary extraction.

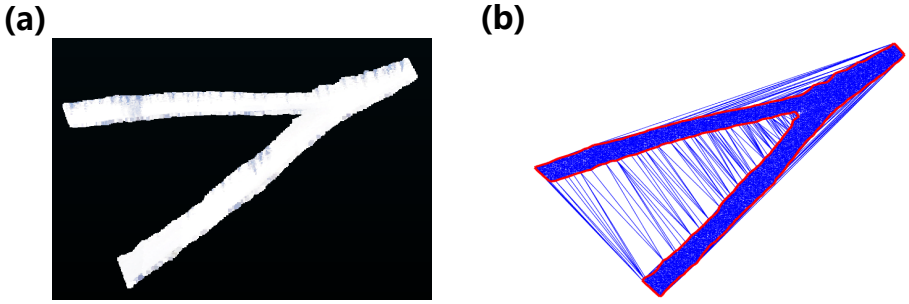

Figure 12. The first group of data-processing results for the Beijing Winter Olympics National Cross-country Skiing Center (Parameters: T = 1.2 cm, A = 0.8, D = 41 cm): (**a**) color point cloud; (**b**) ski-track boundary.

Based on the method presented in this paper, Figure 10 illustrates the processing of the first set of point clouds from the Zhangjiakou Wanlong Ski Resort. Figure 10a shows the extracted 3D point cloud data and Figure 10b shows the boundary line (red line segment) resulting from the triangular mesh; the calculated area of the track was 6294.09 m^2. According to the method proposed in this paper, the second set of point clouds from the Zhangjiakou Wanlong Ski Resort processed are presented in Figure 11. It is shown in Figure 11a that the 3D point cloud data was extracted, and, in Figure 11b, that the boundary line (red line segment) was extracted after the triangular mesh was created, with the area calculated as 3921.18 m^2 using the method proposed in this article. Figure 12 illustrates the processing of the first set of point cloud data for the Beijing Winter Olympics National Cross-country Skiing Center. It is shown in Figure 12a that the 3D point

cloud data was extracted, while Figure 12b shows the boundary line (red line segment) that was extracted after the triangular mesh was generated; the calculated area of the track was 1191.98 m^2. As shown in Figure 13, the method proposed in this paper was used to process the second set of cross-country skiing data from the Beijing National Cross-country Skiing Center. In Figure 13a, the extracted 3D point cloud data is shown, and in Figure 13b, the boundary line (red segment) is shown after the triangular mesh was generated; the calculated track area was 316.18 m^2. The triangular mesh generation, boundary extraction, and area calculation of the extracted ski-track point cloud were completed.

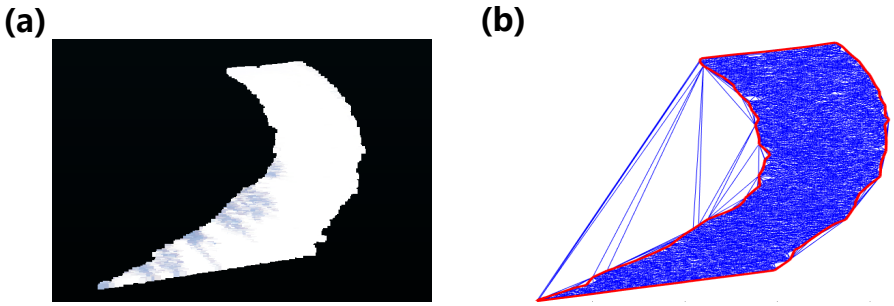

Figure 13. The second group of data-processing results for the Beijing Winter Olympics National Cross-country Skiing Center (Parameters: T = 2.0 cm, A = 0.7, D = 40 cm): (**a**) color point cloud; (**b**) ski-track boundary.

5. Conclusions

In conclusion, in this paper, the RANSAC method was used in order to determine the optimal ski-track plane using the extracted ski-run point clouds [25] (DOI: 10.3390/app12115678). The ski-track point clouds were projected onto the fitting plane to produce a plane point cloud. After constructing the triangular network using the growth algorithm, we proposed an improved algorithm for extracting ski-run boundary points from point clouds to obtain high-precision ski-run edges, connecting them with line segments in order to form polygons. In the final step, the discrete Green's formula was used to calculate the area of the ski track. In order to verify the feasibility and effectiveness of the method, five groups of 10m × 5m test areas on the ski tracks were selected. A comparison of the measurement error offset ratios of the Graham algorithm, the concave hull algorithm, and the algorithm proposed in this paper, produced values of +24.13 percent, +29.28%, and +13.0%, respectively. It can be seen that the method proposed in this paper had the lowest error offset, demonstrating that it represents an improvement and is feasible. Lastly, we used the method proposed in this paper to calculate the ski-run area (based on two sets of point cloud data for the Zhangjiakou Wanlong Ski Resort and two sets of point cloud data for the Beijing Winter Olympic Cross-country Skiing Center), with values obtained of 6294.09 m^2, 3921.18 m^2, 1191.98 m^2 and 316.18 m^2, respectively.

A further analysis of the above-mentioned error offsets indicated that the error offsets calculated by the three methods were all positive, suggesting that the ski-run point cloud extraction was not absolutely accurate. Further research will be conducted on the ski-track extraction method in order to improve its accuracy and correctness in the future.

Author Contributions: Conceptualization, W.W. and H.Z.; methodology, W.W. and C.Z.; software, W.W.; validation, W.W., C.Z. and H.Z.; formal analysis, W.W.; investigation, W.W.; resources, C.Z.; data curation, W.W.; writing—original draft preparation, W.W.; writing—review and editing, C.Z.; visualization, W.W.; supervision, C.Z. and H.Z.; project administration, C.Z.; funding acquisition, C.Z. All authors have read and agreed to the published version of the manuscript.

Funding: This research was funded by the National Key R&D Program of China, Special Project of "Science and Technology Winter Olympics" (2018YFF0300802).

Institutional Review Board Statement: Not applicable.

Informed Consent Statement: Not applicable.

Data Availability Statement: Not applicable.

Conflicts of Interest: The authors declare no conflict of interest.

Abbreviations

The following abbreviations are used in this manuscript:

RANSAC	Random Sample Consensus
2D and 3D	2 Dimensions and 3 Dimensions
MODIS	Moderate Resolution Imaging Spectroradiometer
AVIRIS	Airborne Visible/Infrared Imaging Spectrometer
Modis	Moderate-Resolution Imaging Spectroradiometer
TIN	Triangular Irregular Network
UAV	Unmanned Aerial Vehicle
LiDAR	Light Detection and Ranging
PCL	Point Cloud Library

References

1. Nordin, S.; Svensson, B. Innovative destination governance: The Swedish ski resort of Åre. *Int. J. Entrep. Innov.* **2007**, *8*, 53–66. [CrossRef]
2. Ormiston, D.; Gilbert, A.; Manning, R.E. Indicators and standards of quality for ski resort management. *J. Travel Res.* **1998**, *36*, 35–41. [CrossRef]
3. Goncalves, O. Efficiency and productivity of French ski resorts. *Tour. Manag.* **2013**, *36*, 650–657. [CrossRef]
4. Brachmann, E.; Rother, C. Neural-guided RANSAC: Learning where to sample model hypotheses. In Proceedings of the IEEE/CVF International Conference on Computer Vision, Seoul, Republic of Korea, 27–28 October 2019; pp. 4322–4331.
5. Picard, G.; Arnaud, L.; Domine, F.; Fily, M. Determining snow specific surface area from near-infrared reflectance measurements: Numerical study of the influence of grain shape. *Cold Reg. Sci. Technol.* **2009**, *56*, 10–17. [CrossRef]
6. Liang, T.G.; Huang, X.D.; Wu, C.X.; Liu, X.Y.; Li, W.L.; Guo, Z.G.; Ren, J.Z. An application of MODIS data to snow cover monitoring in a pastoral area: A case study in Northern Xinjiang, China. *Remote Sens. Environ.* **2008**, *112*, 1514–1526. [CrossRef]
7. Tsuyuzaki, S. Environmental deterioration resulting from ski-resort construction in Japan. *Environ. Conserv.* **1994**, *21*, 121–125. [CrossRef]
8. Faria, D.; Pomeroy, J.; Essery, R. Effect of covariance between ablation and snow water equivalent on depletion of snow-covered area in a forest. *Hydrol. Process.* **2000**, *14*, 2683–2695. [CrossRef]
9. Kulkarni, A.V.; Rathore, B.; Singh, S. Distribution of seasonal snow cover in central and western Himalaya. *Ann. Glaciol.* **2010**, *51*, 123–128. [CrossRef]
10. Matzl, M.; Schneebeli, M. Measuring specific surface area of snow by near-infrared photography. *J. Glaciol.* **2006**, *52*, 558–564. [CrossRef]
11. Taillandier, A.S.; Domine, F.; Simpson, W.R.; Sturm, M.; Douglas, T.A.; Severin, K. Evolution of the snow area index of the subarctic snowpack in central Alaska over a whole season. Consequences for the air to snow transfer of pollutants. *Environ. Sci. Technol.* **2006**, *40*, 7521–7527. [CrossRef] [PubMed]
12. Uysal, M.; Howard, G.; Jamrozy, U. An application of importance-performance analysis to a ski resort: A case study in North Carolina. *Visions Leis. Bus.* **1991**, *10*, 4.
13. Faullant, R.; Matzler, K.; Füller, J. The impact of satisfaction and image on loyalty: The case of Alpine ski resorts. *Manag. Serv. Qual. Int. J.* **2008**, *18*, 163–178. [CrossRef]
14. Proksch, M.; Löwe, H.; Schneebeli, M. Density, specific surface area, and correlation length of snow measured by high-resolution penetrometry. *J. Geophys. Res. Earth Surf.* **2015**, *120*, 346–362. [CrossRef]
15. Xu, H.; Bailey, J.; Barrett, E.; Kelly, R. Monitoring snow area and depth with integration of remote sensing and GIS. *Int. J. Remote Sens.* **1993**, *14*, 3259–3268. [CrossRef]
16. Gallet, J.C.; Domine, F.; Zender, C.S.; Picard, G. Measurement of the specific surface area of snow using infrared reflectance in an integrating sphere at 1310 and 1550 nm. *Cryosphere* **2009**, *3*, 167–182. [CrossRef]
17. Kelly, R.E.; Chang, A.T.; Tsang, L.; Foster, J.L. A prototype AMSR-E global snow area and snow depth algorithm. *IEEE Trans. Geosci. Remote Sens.* **2003**, *41*, 230–242. [CrossRef]
18. Domine, F.; Taillandier, A.S.; Simpson, W.R. A parameterization of the specific surface area of seasonal snow for field use and for models of snowpack evolution. *J. Geophys. Res. Earth Surf.* **2007**, *112*, F02031. [CrossRef]
19. Painter, T.H.; Rittger, K.; McKenzie, C.; Slaughter, P.; Davis, R.E.; Dozier, J. Retrieval of subpixel snow covered area, grain size, and albedo from MODIS. *Remote Sens. Environ.* **2009**, *113*, 868–879. [CrossRef]
20. Painter, T.H.; Dozier, J.; Roberts, D.A.; Davis, R.E.; Green, R.O. Retrieval of subpixel snow-covered area and grain size from imaging spectrometer data. *Remote Sens. Environ.* **2003**, *85*, 64–77. [CrossRef]

21. Huang, L.; Li, Z.; Zhou, J.M.; Zhang, P. An automatic method for clean glacier and nonseasonal snow area change estimation in High Mountain Asia from 1990 to 2018. *Remote Sens. Environ.* **2021**, *258*, 112376. [CrossRef]
22. Xiong, Z.; Ji, Z.; Wu, X. Development of a cyclone separator with high efficiency and low pressure drop in axial inlet cyclones. *Powder Technol.* **2014**, *253*, 644–649. [CrossRef]
23. Aghelpour, P.; Guan, Y.; Bahrami-Pichaghchi, H.; Mohammadi, B.; Kisi, O.; Zhang, D. Using the MODIS sensor for snow cover modeling and the assessment of drought effects on snow cover in a mountainous area. *Remote Sens.* **2020**, *12*, 3437. [CrossRef]
24. Donglai, C.; Lihua, L.; Jinglan, Z. A New Index of Stand Density-the Crown Volume Index. *J. Northeast For. Univ.* **2003**, *31*, 15–17.
25. Wang, W.; Zhao, C.; Zhang, H. A New Method of Ski Tracks Extraction Based on Laser Intensity Information. *Appl. Sci.* **2022**, *12*, 5678. [CrossRef]
26. Chum, O.; Matas, J.; Kittler, J. Locally optimized RANSAC. In Proceedings of the Joint Pattern Recognition Symposium, Magdeburg, Germany, 10–12 September 2003; pp. 236–243.
27. Schlimmer, J.C.; Fisher, D. A case study of incremental concept induction. In Proceedings of the AAAI, Philadelphia, PA, USA, 11–15 August 1986; Volume 86, pp. 496–501.
28. Kong, X.; Everett, H.; Toussaint, G. The Graham scan triangulates simple polygons. *Pattern Recognit. Lett.* **1990**, *11*, 713–716. [CrossRef]
29. Flowers, K.R. String wrapping versus massage for reducing digital volume. *Phys. Ther.* **1988**, *68*, 57–59. [CrossRef] [PubMed]
30. Cuppen, J.J. A divide and conquer method for the symmetric tridiagonal eigenproblem. *Numer. Math.* **1980**, *36*, 177–195. [CrossRef]
31. Xu, J.Z.; Wan, Y.C.; Yao, F. A method of 3d building boundary extraction from airborne lidar points cloud. In Proceedings of the 2010 Symposium on Photonics and Optoelectronics, Chengdu, China, 19–21 June 2010; pp. 1–4.
32. Camelli, F.; Lien, J.M.; Shen, D.; Wong, D.W.; Rice, M.; Löhner, R.; Yang, C. Generating seamless surfaces for transport and dispersion modeling in GIS. *Geoinformatica* **2012**, *16*, 307–327. [CrossRef]
33. De Floriani, L.; Mirra, D.; Puppo, E. Extracting contour lines from a hierarchical surface model. In Proceedings of the Computer Graphics Forum, Barcelona, Spain, 6–10 September 1993; Volume 12, pp. 249–260.
34. Zhao, M.; Jiang, L.; Wang, C.; Yang, C.; Yang, X. On the topographic entity-oriented digital elevation model construction method for urban area land surface. *Front. Earth Sci.* **2021**, *15*, 580–594. [CrossRef]
35. Baddeley, A.; Gundersen, H.J.G.; Cruz-Orive, L.M. Estimation of surface area from vertical sections. *J. Microsc.* **1986**, *142*, 259–276. [CrossRef]
36. Schickler, W.; Thorpe, A. Surface estimation based on LIDAR. In Proceedings of the ASPRS Annual Conference, St Louis, MO, USA, 23–27 April 2001; pp. 23–27.
37. Lakhote, A.; Thakkar, M.; Kandregula, R.S.; Jani, C.; Kothyari, G.C.; Chauhan, G.; Bhandari, S. Estimation of active surface deformation in the eastern Kachchh region, western India: Application of multi-sensor DInSAR technique. *Quat. Int.* **2021**, *575*, 130–140. [CrossRef]
38. Chung, F.; Yau, S.T. Discrete Green's functions. *J. Comb. Theory Ser. A* **2000**, *91*, 191–214. [CrossRef]

Disclaimer/Publisher's Note: The statements, opinions and data contained in all publications are solely those of the individual author(s) and contributor(s) and not of MDPI and/or the editor(s). MDPI and/or the editor(s) disclaim responsibility for any injury to people or property resulting from any ideas, methods, instructions or products referred to in the content.